Manuscript prepared for Ocean Sci. Discuss.
with version 4.0 of the LaTeX class copernicus_discussions.cls.
Date: 10 June 2013

A practical scheme to introduce explicit tidal forcing into an OGCM

Kei Sakamoto, Hiroyuki Tsujino, Hideyuki Nakano, Mikitoshi Hirabara, and Goro Yamanaka

Oceanographic Research Department, Meteorological Research Institute, Nagamine, Tsukuba, Ibaraki 305-0052, Japan

Correspondence to: K. Sakamoto
(ksakamot@mri-jma.go.jp)

Abstract

A practical scheme is proposed to introduce tides explicitly into ocean general circulation models (OGCM). In this scheme, barotropic linear response to the tidal forcing is calculated by the time differential equations modified for ocean tides, instead of the original barotropic equations of an OGCM. This allows usage of various parameterizations specified for tides, such as the self attraction / loading (SAL) effect and energy dissipation due to internal tides, without unintentional violation of the original dynamical balances in an OGCM. Meanwhile, secondary nonlinear effects of tides, e.g. excitation of internal tides and advection by tidal currents, are fully represented in the framework of the original OGCM equations. That is, this scheme drives the OGCM by the barotropic linear tidal currents which are predicted progressively by a tuned tide model, instead of the equilibrium tide potential, without large additional numerical costs. We incorporated this scheme into Meteorological Research Institute Community Ocean Model and executed test experiments with a low-resolution global model. The results showed that the model can simulate both of the non-tidal circulations and tidal motion simultaneously. Owing to usage of tidal parameterizations such as a SAL term, a root-mean-squared error in the tidal heights is found to be as small as 10.0 cm, which is comparable to tide models tuned elaborately. In addition, analysis of the speed and energy of the barotropic tidal currents is found to be consistent with past tide studies. The model also showed active excitement of internal tides and tidal mixing. Their impacts should be examined using a model with a finer resolution in future, since explicit and precise introduction of tides into an OGCM is a significant step toward the improvement of ocean models.

1 Introduction

Recent advances in theories of ocean general circulations and observations of deep seas have revealed that tides play a significant role in open oceans, as well as in coastal areas. As a representative study, Munk and Wunsch (1998) suggested that vertical mixing in deep seas due to breaking of internal tides is an important process in the global thermohaline circulations. This hypothesis is supported by the fact that a large part of the tidal energy is dissipated in deep seas (Egbert and Ray, 2001; St. Laurent and Garrett, 2002; Niwa and Hibiya, 2011). In addition, various studies reported that local strong tidal mixing affects the ocean circulations on a basin scale. For example, tidal mixing near the Kuril Islands plays an important role in the formation process of the water mass called North Pacific Intermediate Water (Nakamura and Awaji, 2004; Osafune and Yasuda, 2006). Tidal mixing in the Arctic shelf seas modifies the salinity budget through interaction with sea ice, and, as a result, the deep thermohaline circulation in the North Atlantic (Postlethwaite et al., 2011). In a similar fashion, tidal mixing over the Antarctic shelves affects the formation process of Antarctic Bottom Water (Robertson, 2001a,b; Pereira et al., 2002). These studies suggest an influence of tides on the general circulation.

However, only recently have tides begun to be sufficiently taken into account in ocean general circulation models (OGCMs). One reason is that most of them could not represent tides since they adopted the rigid-lid condition to preclude the surface gravity waves due to the CFL condition. Another is that tidal motions with a time scale of half or one day were omitted intentionally to focus on variations with longer time scales in geostrophic currents. Recently, effects of tides have begun to be considered in OGCMs, stimulated by advances in the studies of tides.

The methodology to incorporate tides into OGCMs is classified into two types, i.e. an implicit one and an explicit one. The implicit type uses indirect parameterizations about tidal effects rather than simulating tides themselves, to avoid drastic change of the OGCM framework. A typical parameterization adopted by various recent OGCMs is mixing enhancement in deep seas and coastal areas (e.g. St. Laurent and Garrett, 2002). Lee et al. (2006) reported that this kind of parameterization contributes to good representation of the salinity distribution in the North Atlantic. As another indirect parameterization, Bessiéres et al. (2008) proposed an implicit parameterization for the tidal residual currents.

The explicit type introduces the tidal dynamics into free-surface OGCMs directly; i.e., through introduction of tidal forcing in the momentum equations. Though this type needs large computer resources and modification of a part of the OGCM framework, some achievements have been already reported. For example, Schiller and Fiedler (2007) improved model representation of water transport and mixing in the Indonesian Through Flow region and Australian shelves.

Müller et al. (2010) reported improvement in modeling of the pathway of the North Atlantic Current and water-modification processes in the North Atlantic. In addition, Arbic et al. (2010) discussed a possibility that explicit incorporation of tides into an eddy-resolving OGCM may lead to drastic improvement in representation of various ocean processes, such as interaction between meso-scale eddies and tides, form drag on the sea mounts, excitement and propagation of internal tides in realistic three-dimensional stratification. Development of an OGCM, which simultaneously simulates the time evolution of the tidal field and the non-tidal field (called the basic field hereafter), is now a frontier in ocean modeling.

On the other hand, modeling of tides themselves has been developed virtually independently of OGCMs, based on barotropic ocean models. Many modeling studies have shown that dynamics particular to tides need to be introduced into the model equations for accurate representation of tides (e.g. Matsumoto et al., 2000). A typical example is the self attraction / loading (SAL) effect. This represents modification of the gravity field and elastic deformation of the bottom ground induced by movement of ocean water (Schwiderski, 1980). Due to the SAL effect, the pressure gradient term accompanied by the tidal height gradient, -g $\nabla\eta$, is modified in the equation of barotropic motion as follows

$$-g\nabla(\eta-\eta_{\mathrm{SAL}}). \tag{1}$$

In order to represent the gravity change of the self attraction and the loading effect, which is that the sea surface elevation induced by convergence of barotropic velocities is cancelled partly by depression of the bottom ground due to water weight, the elevation is subtracted by η_{SAL} in calculation of the pressure gradient. Though various evaluations of η_{SAL} have been proposed, a linear response is used as a first-order approximation

$$\eta_{\mathrm{SAL}}=(1-\alpha)\eta, \tag{2}$$

where α is a constant between 0.88 and 0.95 (Matsumoto et al., 2000). Under this approximation of the SAL term, which has been traditionally referred to as the ”scalar approximation” (Hendershott, 1972), the pressure gradient term $-g\nabla\eta$ is modified into $-g\alpha\nabla\eta$.

Another issue of tide modeling is energy dissipation of tides, such as energy transfer to internal tides and form drag by bottom topography on tidal currents. In general, as model resolution becomes finer, a model can represent more kinds of dissipation processes without parameterization. However, considering that internal tide processes cannot be reproduced sufficiently even in a model with a horizontal resolution of 10 km, which is considerably fine at present (e.g. Niwa and Hibiya, 2011), a parameterization specialized for dissipation is still necessary to represent tides with good accuracy (Jayne and St. Laurent, 2001; Arbic et al., 2004). Furthermore, various parameterizations unusual for OGCMs have been proposed for tidal modeling, such as body tides, which are included here, and atmospheric tides. See Chapter 6 of Kantha and Clayson (2000) for detail.

The knowledge obtained by tidal modeling studies should be exploited in order to introduce tides into OGCMs with high accuracy. However, this is a difficult task, since dynamical balances in the basic field of OGCMs are violated if terms proposed for tidal modeling are incorporated into the OGCM equations directly (Arbic et al., 2010). For example, the SAL term of Eq. (1) changes the geostrophic relationship between sea surface gradient and currents. Parameterizations for dissipation of tidal currents are not suited for the geostrophic currents in OGCMs either, since their time scales of change are so different that their dissipation mechanisms are not the same. Therefore, we cannot simply replace the governing equations of OGCMs by those of tidal modeling. The two sets of the governing equations should be harmonized by some means to introduce tides into an OGCM.

This problem has not been solved yet. In most of the model studies introducing tides explicitly into OGCMs, the equilibrium tidal potential is given directly through the free-surface barotropic equation of motion, and the tidal and basic fields are calculated without separation (Thomas et al., 2001; Schiller, 2004; Schiller and Fiedler, 2007; Müller et al., 2010). In these studies, the problem due to the differences between the tidal and basic (geostrophic and eddying) characteristics is not investigated sufficiently. To the best of our knowledge, Arbic et al. (2010), who introduced tides into an eddy-resolving global OGCM, examined this problem most carefully. Though they calculated time evolution of the tidal and basic fields without separation as in other studies, they elaborated a method to prevent the parameterizations specialized for tides from affecting the basic fields. Specifically, they defined the tidal currents as velocity deviation from 25-hour running mean, which is calculated progressively in the model, and restricted the tidal dissipation parameterization to work on the tidal currents only. In addition, they defined the tidal height as sea surface height (SSH) deviation from the dynamical height, which is calculated every time step, and evaluated the SAL term so that the SAL would not contaminate the basic field (e.g. geostrophic currents). However, their method is expected to expend a substantial amount of numerical resources. Furthermore, it seems questionable that all of the SSH deviation is treated as the tidal height.

As a solution to the aforementioned problem, we propose a new practical scheme to incorporate tides explicitly into OGCMs. This scheme is based on the recognition that the governing equations are different between the tidal and basic fields, and calculates their time evolutions separately. This approach is in contrast to traditional typical schemes such as Schiller (2004) where the tidal and basic fields are given by the same governing equations.

First, this paper will explain the scheme in detail. Next, model representations of tides by this scheme will be shown based on some test experiments of a global OGCM. Finally, tidal effects on the basic fields in the OGCM will be presented briefly.

2 Scheme and model

2.1 Conventional scheme

Before presenting the new tide scheme, we show the scheme of Schiller (2004) as a representative example of the traditional schemes where the tidal forcing is incorporated directly into the governing equations. First, the original standard expressions of the barotropic equations of motion and continuity are

$$\frac{\partial \boldsymbol{U}}{\partial t} + f\boldsymbol{k} \times \boldsymbol{U} = -g(\eta + H)\nabla\eta + \boldsymbol{D} + \boldsymbol{\tau}^{\mathrm{btm}} + \boldsymbol{X} \tag{3}$$

$$\frac{\partial \eta}{\partial t} + \nabla \cdot \boldsymbol{U} = F_w, \tag{4}$$

where $\boldsymbol{U}$ is the vertically integrated transport vector [m^2 s^{-1}], η the SSH anomaly [m], f the Coriolis parameter [s^{-1}], $\boldsymbol{k}$ the upward vertical unit vector [dimensionless], g the gravitational acceleration [m s^{-2}], H the water depth [m], $\boldsymbol{D}$ a dissipation parameterization [m^2 s^{-2}], τ^{btm} the bottom friction (already divided by standard density) [m^2 s^{-2}], $\boldsymbol{X}$ the other residual terms including the vertically integrated advection and the wind stress [m^2 s^{-2}], and F_w is the surface freshwater flux [m s^{-1}]. Introduction of tides means that the equilibrium tidal potential η_0 and the SAL term η_{SAL} are added, and $\boldsymbol{D}$ is changed to the dissipation parameterization specialized for tides, which is indicated by $\boldsymbol{D}_{\mathrm{modified}}$, as

$$\frac{\partial \boldsymbol{U}}{\partial t} + f\boldsymbol{k} \times \boldsymbol{U} = -g(\eta + H)\nabla\left(\eta - \beta\eta_0 - \eta_{\mathrm{SAL}}\right) + \boldsymbol{D}_{\mathrm{modified}} + \boldsymbol{\tau}^{\mathrm{btm}} + \boldsymbol{X}, \tag{5}$$

where β represents the body tide effect (Schwiderski, 1980). If the scalar approximation for the SAL term, Eq. (2), is adopted, Eq. (5) becomes

$$\frac{\partial \boldsymbol{U}}{\partial t} + f\boldsymbol{k} \times \boldsymbol{U} = -g(\eta + H)\nabla\left(\alpha\eta - \beta\eta_0\right) + \boldsymbol{D}_{\mathrm{modified}} + \boldsymbol{\tau}^{\mathrm{btm}} + \boldsymbol{X}. \tag{6}$$

This is equivalent to a standard barotropic tidal model, e.g. the continuous ocean tide equations of Schwiderski (1980). In this traditional scheme, the time evolutions of $\boldsymbol{U}$ and η under the tidal forcing are obtained by solving Eqs. (4) and (5) (or (6)) under $\eta_0(x, y, t)$, which is analytically calculated.

This scheme works well in modeling tides without the basic circulation. However, in modeling of the tidal and basic fields simultaneously, it induces the problem that the terms specialized for tides affect the basic fields unintentionally. In fact, Eq.(6) shows clearly that the SAL term changes the relationship between the sea surface gradient and the barotropic currents. The dissipation $\boldsymbol{D}_{\mathrm{modified}}$ also changes the basic currents. Introduction of parameterizations specified for tides results in violation of the dynamical balances in the basic fields.

2.2 New scheme

The violation of the dynamical balance in the basic fields arises from the fact that the barotropic equation of motion for tides Eq.(5) is different from the OGCM standard equation for the basic fields Eq.(3). Therefore, our new tide scheme calculates the tidal and basic fields by two different equations as explained below. The objective of our new scheme is to simultaneously achieve both of accurate modeling of the tides and maintenance of the dynamical balances in the original OGCM.

The basis of the scheme is decomposition of the variables, $\boldsymbol{U}$, η, $\boldsymbol{D}$ and $\boldsymbol{\tau}^{\mathrm{btm}}$ in the barotropic equations into the linear tidal component and the basic component,

$$\boldsymbol{U} = \boldsymbol{U}_b + \boldsymbol{U}_{lt} \tag{7}$$

$$\eta = \eta_b + \eta_{lt} \tag{8}$$

$$\boldsymbol{D} = \boldsymbol{D}_b + \boldsymbol{D}_{lt} \tag{9}$$

$$\boldsymbol{\tau}^{\mathrm{btm}} = \boldsymbol{\tau}_b^{\mathrm{btm}} + \boldsymbol{\tau}_{lt}^{\mathrm{btm}}. \tag{10}$$

The linear tidal component indicated by the subscript, 'lt,' corresponds to the primary response of the barotropic ocean to the equilibrium tide potential. The basic component with the subscript, 'b,' corresponds to the other barotropic and baroclinic motions, including all of the dynamical processes in the original OGCM and the secondary effects of tides (e.g. internal tides, tidal advection, bottom shear of tidal currents and so on). There are some difficulties posed by the decomposition of the variables, especially $\boldsymbol{\tau}^{\mathrm{btm}}$, and the decomposition is discussed in more detail later.

Each of the two components is calculated using its own governing equation. The linear tidal component is governed by the equations for tidal modeling; i.e. a modified Eq.(5) and continuity equation,

$$\frac{\partial \boldsymbol{U}_{lt}}{\partial t} + f\boldsymbol{k} \times \boldsymbol{U}_{lt} = -g(\eta + H)\nabla\left(\eta_{lt} - \beta\eta_0 - \eta_{\mathrm{SAL}}\right) + \boldsymbol{D}_{lt} + \boldsymbol{\tau}_{lt}^{\mathrm{btm}} \tag{11}$$

$$\frac{\partial \eta_{lt}}{\partial t} + \nabla \cdot \boldsymbol{U}_{lt} = 0. \tag{12}$$

The basic component is governed by the standard OGCM equations, i.e. Eqs. (3) and (4)

$$\frac{\partial \boldsymbol{U}_b}{\partial t} + f\boldsymbol{k} \times \boldsymbol{U}_b = -g(\eta + H)\nabla \eta_b + \boldsymbol{D}_b + \boldsymbol{\tau}_b^{\mathrm{btm}} + \boldsymbol{X} \tag{13}$$

$$\frac{\partial \eta_b}{\partial t} + \nabla \cdot \boldsymbol{U}_b = F_w. \tag{14}$$

The numerical procedure to predict the two components by the above equations is schematically illustrated by Fig. 1. Generally in a free-surface OGCM, starting from velocity $\boldsymbol{u}$ and SSH η at the time step N, those at the next step $N+1$ are calculated using the equations of motion and continuity, and usually the barotropic and baroclinic constituents are predicted differently in the calculation (so called mode splitting, indicated by $\hat{\boldsymbol{u}}$, $\boldsymbol{U}$ and η in Fig. 1). The key of our new scheme is to split the barotropic constituent into the basic and linear tidal components, further ($\boldsymbol{U}_b, \eta_b, \boldsymbol{U}_{lt}$ and η_{lt}), and to calculate the time evolution of $\boldsymbol{U}_{lt}$ and η_{lt} separately from $\boldsymbol{U}_b$ and η_b. The solid arrow related to $\boldsymbol{U}_{lt}$ and η_{lt} in Fig. 1 indicates this independent calculation, while the dashed arrow means that $\boldsymbol{U}_b$ and η_b are given by subtraction, i.e. $\boldsymbol{U} - \boldsymbol{U}_{lt}$ and $\eta - \eta_{lt}$, respectively. That is, the three sets of the governing equations are calculated at each time step, and the three-dimensional velocity field at the next step is determined by their summation.

The linear terms in the barotropic equations, such as the Coriolis force and the Laplacian horizontal viscosity, can be split into the basic and linear tidal components naturally, while the non-linear terms need to be treated more carefully. In our scheme, all of the advection terms are incorporated into the basic equations ($\boldsymbol{X}$ in Eq. (13)), and the linear tidal equations have no advection. Specifically, the tracer and momentum advections are calculated using the three-dimensional velocity field, given by the summation of all of their components ($\boldsymbol{u}$ in Fig.1), and their sums are added to the basic equations. This is based on the assumption of the scheme: the linear tidal component represents only the linear primary response to the tidal forcing, and the other secondary effects, such as tidal advection and internal tides, are represented by the basic component. Modification of the tides due to interaction between tidal currents and basic fields is also represented by the basic equations as secondary oscillations with tidal frequencies (see Appendix for detail).

The wind stress (included in $\boldsymbol{X}$) and the freshwater flux F_w are also left in the original OGCM equations, Eqs. (13) and (14). This is because the wind-induced circulations and the thermohaline circulations induced by these terms should be represented in the OGCM framework. If these terms were moved to the linear tidal equations, the dynamical balance would be violated due to tidal parameterizations such as the SAL term. In addition, it has not been reported that these terms change the primary response of the ocean to the tidal forcing, as far as we know. On the other hand, various processes of secondary interaction between tides and basic fields have been reported, e.g. influence of tidal mixing on a thermohaline circulation (Lee et al., 2006), modification of internal tides induced by winds (Xing and Davies, 1997), and this kind of interaction processes is intended to be represented under the OGCM equations.

Decomposition of the bottom friction $\boldsymbol{\tau}^{\mathrm{btm}}$ should be carefully treated, since it is non-linear, when expressed by a quadratic form as (Taylor, 1920; Weatherly et al., 1980)

$$\boldsymbol{\tau}^{\mathrm{btm}} = -C_D \left| \frac{\boldsymbol{U}}{H+\eta} \right| T_\theta \frac{\boldsymbol{U}}{H+\eta}. \tag{15}$$

The constant C_D indicates a drag coefficient and T_θ a matrix representing horizontal veering,

$$T_\theta = \begin{pmatrix} \cos\theta & -\sin\theta \\ \sin\theta & \cos\theta \end{pmatrix}, \tag{16}$$

where θ is the veer angle. (The unit of $\boldsymbol{\tau}^{\mathrm{btm}}$ is $\mathrm{m}^2\ \mathrm{s}^{-2}$, and C_D and T_θ are dimensionless.) There are various ways to split Eq. (15) into the term for the basic barotropic equation and that for the linear tidal equation. For simplicity of the equations, we decided that a sum of the two components is used for $|\boldsymbol{U}/(H+\eta)|$ (the coefficient part), but each component for $\boldsymbol{U}/(H+\eta)$ (the vector part) is given by

$$\boldsymbol{\tau}_b^{\mathrm{btm}} = -C_D \left| \frac{\boldsymbol{U}_b + \boldsymbol{U}_{lt}}{H+\eta} \right| T_\theta \frac{\boldsymbol{U}_b}{H+\eta} \tag{17}$$

$$\boldsymbol{\tau}_{lt}^{\mathrm{btm}} = -C_D \left| \frac{\boldsymbol{U}_b + \boldsymbol{U}_{lt}}{H+\eta} \right| T_\theta \frac{\boldsymbol{U}_{lt}}{H+\eta}. \tag{18}$$

It should be noted that $\boldsymbol{\tau}_{lt}^{\rm btm}$ depends on $\boldsymbol{U}_b$ through the coefficient part. In open oceans, it is guessed that this dependency is not important, since both of the barotropic velocities $\boldsymbol{U}_b/(H+\eta)$ and $\boldsymbol{\tau}_{lt}^{\rm btm}$ itself are generally small. However in coastal regions, since they become large, the reproducibility of the tides may be affected to some extent. (We investigated the affect using our low-resolution model by replacing the coefficient part of Eq. (18) by $|\boldsymbol{U}_{lt}/(H+\eta)|$. In a one-year experiment, change of the tidal heights is found to be 1% at most.) Through the decomposition, we make the linear tidal equations, Eqs. (11) and (12), as simple as possible to only represent the primary barotropic response to the tidal forcing.

Using our new scheme, we can avoid the violation of the dynamical balance in the basic field. To show this achievement more clearly, we assume the SAL term has a linear form as $\eta_{\rm SAL} \sim (1-\alpha)\eta_{lt}$ and sum Eqs. (13) and (11) to find that

$$\frac{\partial \boldsymbol{U}}{\partial t} + f\boldsymbol{k}\times\boldsymbol{U} = -g(\eta+H)\nabla\left(\eta_b+\alpha\eta_{lt}-\beta\eta_0\right)+\boldsymbol{D}_b+\boldsymbol{D}_{lt}+\boldsymbol{\tau}_b^{\rm btm}+\boldsymbol{\tau}_{lt}^{\rm btm}+\boldsymbol{X}. \qquad (19)$$

This equation of motion clearly changes from the conventional scheme, Eq. (6). The SAL effect (α) works on η_{lt} only, the body tide effect works on the equilibrium tide only, and the expressions for dissipation and bottom friction for tides ($\boldsymbol{D}_{lt}$ and $\boldsymbol{\tau}_{lt}^{\rm btm}$) are different from the basic field ($\boldsymbol{D}_b$ and $\boldsymbol{\tau}_b^{\rm btm}$). As a result, when tides are omitted (i.e. $\eta_0 \equiv 0$), $\boldsymbol{U}_{lt}, \eta_{lt}, \boldsymbol{D}_{lt}$ and $\boldsymbol{\tau}_{lt}^{\rm btm}$ are permanently zero from Eqs. (11), (12) and (18), so that Eq. (19) becomes identical to the original barotropic equation, Eq. (3). Thus, introduction of our tide scheme does not modify the basic equations in contrast to conventional tide schemes.

From the point of view of tidal modeling, our scheme enables us to tune the parameterizations of tides independently of the dynamical balance in the basic field. The value of α, the formulation of $\boldsymbol{\tau}_{lt}^{\rm btm}$ and the parameterization of $\boldsymbol{D}_{lt}$ can be selected independently.

To clarify the base of the new scheme, the meaning of ”the linear tidal component” is noted again here. Strictly speaking, a part of the basic component of η is used in Eqs. (11) and (12) so the linear tidal component is not strictly independent of the basic component. However, the linear tidal component is treated separately from the basic component. In other words, the scheme calculates the linear tidal currents under the equilibrium tidal potential progressively, and uses it as a model forcing, instead of introducing the potential to the model directly. That is, the linear tidal component can be referred to as an external forcing for the model, rather than the tidal field reproduced in the model. To see the tidal field precisely, secondary oscillations with tidal frequencies in the basic field need to be taken into account, as explained in Appendix.

In closing this subsection, the practical approximation used by our new scheme is discussed in detail in comparison to the scheme of Arbic et al. (2010). The first principle of our new scheme is the fact that the different sets of the governing equations should be applied to the tidal component and the non-tidal component separately, in order to introduce tides into OGCMs realistically. And, to do so, we have to carry out decomposition of the two components in an OGCM. In an ideal scheme, the tidal component would represent all of the barotropic motions which oscillate with tidal frequencies and have the spatial structures corresponding to the tidal forcing, while the non-tidal component would represent all of the other motions. Hereafter, we call them ”the ideal tidal component” and ”the ideal basic component”, respectively. Under such an ideal decomposition, the barotropic equation comparable to Eq. (19) becomes

$$\frac{\partial \boldsymbol{U}}{\partial t} + f\boldsymbol{k}\times\boldsymbol{U} = -g(\eta+H)\nabla\left(\eta_{\mathrm{IB}}+\alpha\eta_{\mathrm{IT}}-\beta\eta_0\right)+\boldsymbol{D}_{\mathrm{IB}}+\boldsymbol{D}_{\mathrm{IT}}+\boldsymbol{\tau}_{\mathrm{IB}}^{\mathrm{btm}}+\boldsymbol{\tau}_{\mathrm{IT}}^{\mathrm{btm}}+\boldsymbol{X}_{\mathrm{IB}}+\boldsymbol{X}_{\mathrm{IT}}, \tag{20}$$

where the variables with the subscripts of ”IB” and ”IT” indicate the ideal basic component and the ideal tidal component, respectively. However, it is virtually impossible to extract the ideal tidal component, i.e. all of the motions with tidal frequencies and with spatial patterns corresponding to the tidal forcing, from changing model results. A certain approximation is necessary for the decomposition.

In the scheme of Arbic et al. (2010), the decomposition is executed in a straightforward manner. They approximated terms in Eq. (20) as follows

$$\begin{cases} \eta_{\mathrm{IB}} = \eta_{\mathrm{dynamic-height}} \\ \eta_{\mathrm{IT}} = \eta - \eta_{\mathrm{dynamic-height}} \\ \boldsymbol{D}_{\mathrm{IB}} = \boldsymbol{D}_{\mathrm{25h-mean-current}} \\ \boldsymbol{D}_{\mathrm{IT}} = \boldsymbol{D}_{\mathrm{anomaly-current}} \end{cases}, \tag{21}$$

where $\eta_{\mathrm{dynamic-height}}$ indicates the dynamic height anomaly, $\boldsymbol{D}_{\mathrm{25h-mean-current}}$ the viscosity for the 25-hour mean currents, and $\boldsymbol{D}_{\mathrm{anomaly-current}}$ the viscosity for the anomalous currents. It is guessed that the bottom friction $\boldsymbol{\tau}^{\mathrm{btm}}$ and the other (non-linear) term $\boldsymbol{X}$ are formulated in the same manner for the two components. In an OGCM with the Arbic et al. (2010) tide scheme, Eq. (20) is calculated under these approximations.

Meanwhile, our new scheme approximates terms of Eq. (20) as follows

$$\begin{cases} \eta_{\mathrm{IB}} = \eta_b = \eta - \eta_{lt} \\ \eta_{\mathrm{IT}} = \eta_{lt} \\ \boldsymbol{D}_{\mathrm{IB}} = \boldsymbol{D}_b \quad (\text{for } \boldsymbol{U}_b = \boldsymbol{U} - \boldsymbol{U}_{lt}) \\ \boldsymbol{D}_{\mathrm{IT}} = \boldsymbol{D}_{lt} \quad (\text{for } \boldsymbol{U}_{lt}) \\ \boldsymbol{\tau}_{\mathrm{IB}}^{\mathrm{btm}} = \boldsymbol{\tau}_b^{\mathrm{btm}} \quad (\text{for } \boldsymbol{U}_b) \\ \boldsymbol{\tau}_{\mathrm{IT}}^{\mathrm{btm}} = \boldsymbol{\tau}_{lt}^{\mathrm{btm}} \quad (\text{for } \boldsymbol{U}_{lt}) \\ \boldsymbol{X}_{\mathrm{IB}} = \boldsymbol{X} \quad (\text{for } \boldsymbol{U}_b + \boldsymbol{U}_{lt}) \\ \boldsymbol{X}_{\mathrm{IT}} = 0 \end{cases}, \tag{22}$$

by introducing the barotropic linear tidal component, η_{lt} and $\boldsymbol{U}_{lt}$, and the equations to calculate their time evolution, Eqs. (11) and (12). That is, the practical approximation of our new scheme is to use the solution of a linear tidal model in the decomposition. It is because of this approximation that tidal fields can be reproduced with less numerical resources and be accurate enough to represent tidal effects in an OGCM, as shown in Sect. 3. However, it may be difficult to reproduce tidal fields in detail in coastal areas, since non-linear effects become important there so that the linear tidal component becomes less representative.

Though relatively small, some numerical resources are expended by the scheme. Since one more barotropic equation needs to be calculated as shown in Fig. 1, the numerical cost of the barotropic calculation doubles. For our test experiment, the computational time increased by 4% as a whole.

2.3 Model

Test experiments of our tide scheme were executed using the Meteorological Research Institute Community Ocean Model (MRI.COM) (Tsujino et al., 2010, 2011). The MRI.COM is a hybrid z-σ coordinate free-surface multilevel model which solves the primitive equations under the hydrostatic and Boussinesq approximations, and adopts a barotropic-baroclinic mode splitting technique. The model domain is global (so called tripolar grid coordinates (Murray, 1996)). The horizontal resolution is 1°in the zonal direction and 1/2°in the meridional direction, except for the Arctic region. The model has 50 levels in the vertical direction with layer thickness increasing from 4 m at the surface to 600 m at 6300-m depth. The model settings are ordinary as recent global OGCMs except for the tide scheme as follows (See (Tsujino et al., 2011) for details). The model uses an isopycnal diffusion, the Second Order Moment tracer advection (Prather, 1986), a harmonic friction with a Smagorinsky-like viscosity (Griffies and Hallberg, 2000), a sea ice model (Mellor and Kantha, 1989; Hunke and Ducowicz, 1997, 2002), a bottom boundary layer scheme (Nakano and Suginohara, 2002), and the Generic Length Scale vertical mixing scheme (Umlauf and Burchard, 2003). The bottom friction for the basic field, $\boldsymbol{\tau}_b^{\mathrm{btm}}$, is represented by the quadratic friction Eq. (15) with $C_D = 0.00125$ and $\theta = 10°$(Weatherly et al., 1980).

Configurations of the tide scheme are rather simple in order to verify its basic features. The SAL term is approximated by the linear form $\eta_{\mathrm{SAL}} = (1-\alpha)\eta_{lt}$ with $\alpha = 0.88$, and the constant β by 0.7. (Strictly speaking, β should depend on the Love numbers (Chapter 6.3 of Kantha and Clayson, 2000).) A simple harmonic horizontal viscosity is used for the diffusivity term, $\boldsymbol{D}_{lt}$, with a coefficient of 6×10^4 m^2 s^{-1}, though more sophisticated parameterizations have been proposed such as a formulation dependent on the mixing length (Schwiderski, 1980). The no-slip condition is imposed at the lateral boundary of the bottom topography, so that the horizontal viscosity works there. The bottom friction for the linear tidal component $\boldsymbol{\tau}_{lt}^{\mathrm{btm}}$ is the quadratic friction with the conventional parameters $C_D = 0.0025$ and $\theta =$ 0 °(Schwiderski, 1980). Thus, $\boldsymbol{\tau}_{lt}^{\mathrm{btm}}$ uses a different parameterization from $\boldsymbol{\tau}_b^{\mathrm{btm}}$, since the Weatherly et al. (1980) scheme used for $\boldsymbol{\tau}_b^{\mathrm{btm}}$ is designed for the turbulent Ekman layer and unsuitable for the tidal currents (Sakamoto and Akitomo, 2008, 2009). The main eight tidal constituents (K1, O1, P1, Q1, M2, S2, N2 and K2) are used for the equilibrium tide potential, and their amplitudes and phases are given after Table 1 of Schwiderski (1980). [1]

2.4 Experimental cases

The test experiments were executed under the following boundary and initial conditions. The atmospheric forcings, such as wind stress, latent and sensible heat fluxes, evaporation and precipitation, were calculated using the interannual dataset of the Coordinated Ocean-ice Reference Experiments (Griffies et al., 2009) and the bulk formulas of Large and Yeager (2004). For spin up, we ran the model without tides over one thousand years under the repeated atmospheric forcings from a state of rest with climatological temperature and salinity, to reach a quasi-steady realistic situation (Tsujino et al., 2011). The instantaneous field on 11 May 2001 was used for the initial condition of the tide experiment. The test period was 40 days, though 10 days in some experimental cases. The time step interval is as short as 3 minutes following Section 4b of Schwiderski (1980).

The seven experiment cases were executed (Table 1). The cases TIDE and NOTIDE were run with the eight tidal constituents and without tide, respectively, and are analyzed in this paper. Results of long integration (one year) are also shown for these two cases. The TIDEa1 case with $\alpha = 1$ is used for comparison with a case in which that the SAL term is ignored without violating dynamical balances in the basic field as in a conventional scheme. [2] The M2 case, which uses the M2 constituent only, and the K1 case, which uses the K1 constituent only, are used for dynamical analysis of tides in the model. The cases M2v2 and M2v10 changing the tidal horizontal viscosity to 2×10^4 m^2 s^{-1} and 10×10^4 m^2 s^{-1}, respectively, are used to examine dependency on the $\boldsymbol{D}_{lt}$ setting. Usage of different values for the horizontal viscosity for the tides as opposed to basic fields is based on Polzin (2008), who proposed an interpreta-

[1] Two misprints were found: the correct astronomical argument of P1 is $-h_0 - 90$, and the day number from the reference date D is $d + 365(y - 1975) + \mathrm{Int}[(\mathrm{y} - 1973)/4]$.

[2] This case does not correspond perfectly to a case using the conventional scheme where tidal and basic fields are treated without separation, since $\boldsymbol{D}_{lt}$ differs from $\boldsymbol{D}_b$.

tion of horizontal viscosity as a way to parameterize the interaction between mesoscale eddies and internal waves. That is, the usage of different values means that mesoscale eddies interact differently with internal waves that result from geostrophic adjustment than with internal tides.

The global tide dataset of Matsumoto et al. (2000) (NAO.99b) was downloaded from web and used to assess model reproducibility of the tidal height. This dataset is a reanalysis product made by assimilation of SSH satellite observations to a barotropic tide model with a horizontal resolution of 0.5 °. Though they reported that errors in tidal height are 2cm at maximum (Figs. 3 and 4 of their paper), the dataset is assumed to be the actual tidal heights in this study.

3 Results

3.1 Tidal height

The test experiments with our tidal scheme successfully reproduced many of the large-scale features known to be in the tidal field as well as basic field. Figure 2a shows the instantaneous field of SSH η at the end of case TIDE. Tides with a basin scale are clearly seen, along with the geostrophic circulation on a large scale, e.g. the meridional gradient of the Antarctic Circumpolar Current.

In this paper, we define the tidal height η_t by the SSH anomaly from case NOTIDE,

$$\eta_t \equiv \eta - \eta(\mathrm{NOTIDE}). \tag{23}$$

Figure 2b and c show η_t and η_{lt} in case TIDE, respectively. As noted in Sect. 2.2, the former represents the whole tidal motion including non-linear effects, while the latter is the primary barotropic response to the tidal forcing following Eqs. (11) and (12). Except for a few differences in coastal areas (10 cm at maximum), they are almost identical globally (Fig. 2d). This result supports our expectation that the linear tidal components, $\boldsymbol{U}_{lt}$ and η_{lt}, represent most of the tidal motions. Only the linear tidal equations adopt parameterizations specified for tides in our new scheme, which here is suggested to be enough to reproduce tides in a global model.

For comparison, Fig. 2e shows the tidal height of the reanalysis dataset (Matsumoto et al., 2000), η_t^a. The patterns of sea surface elevation in η_t(or η_{lt}) of TIDE and η_t^a are very similar in the Indian, Pacific and Atlantic oceans, though there are some differences around the Antarctic continent. Their amplitudes are also very close. For example, the local maximum in the eastern equatorial Pacific region is approximately 87cm in both of η_t and η_t^a. This result suggests that our new scheme worked as expected, so that the model reproduced realistic time evolution of tides.

In contrast, η_t in case TIDEa1, which ignored the SAL term, is different from η_t^a (Fig. 2f). For example, the local maximum in the east Pacific was not located in the equatorial region, but adjacent to the west coast of North America, and the pattern of sea surface elevation around New Zealand deviated anti-clockwise by approximately 60°. The contrasting results between TIDE and TIDEa1 indicate that realistic tides cannot be modeled in an OGCM if the original barotropic equation is used to calculate time evolution of tides. It is necessary to use parameterizations developed for tides. Even the scalar approximation for the SAL term, for example, improves simulations of the tides.

To investigate causes of the differences between TIDE and TIDEa1 in detail, the amplitude of the tidal height variation is evaluated by the root-mean-square of η_t, η_{RMS},

$$\eta_{\mathrm{RMS}} = \left(\frac{1}{T_1 - T_0} \int_{T_0}^{T_1} \eta_t^2 dt \right)^{1/2}, \tag{24}$$

where T_0 and T_1 indicate 5 May 2001 and 20 June 2001, i.e. the times after 10 and 40 days from the experiment start, respectively. Figure 3 shows η_{RMS} in TIDE, TIDEa1 and the assimilation dataset. Comparing η_{RMS}(TIDE) and the assimilation result η_{RMS}^a, the distributions and the local maxima are very similar except for some differences (e.g. η_{RMS} is slightly smaller in the Indian Ocean, and larger in the western equatorial Pacific region). Similarly, η_{RMS}(TIDEa1) is close to η_{RMS}^a, though its distribution seems somewhat distorted. It is discussed in Sect. 3.2 how the viscosity parameterization influences the performance of TIDE as opposed to TIDEa1.

Next, the reproducibility of the tidal phase is examined. As a representative result, Fig. 4 shows a time series of η_t at some location in the equatorial Pacific. In contrast to the amplitudes, the reproducibility of the tidal phase differs substantially between TIDE and TIDEa1. The η_t phase is ahead by up to 1.5 hour from η_t^a in TIDEa1 (corresponding to 45°for semi-diurnal tides), while by only 0.5 hour in TIDE. As a result, the difference between η_t and η_t^a decreases drastically in TIDE, in comparison with TIDEa1. Thus, the problem that the tidal phase is ahead too much in TIDEa1 is corrected to some extent in TIDE. This is one important reason for the difference in the reproducibilities of the two cases shown in Fig. 2.

A possible mechanism of this correction is as follows. Introduction of the SAL term modifies the gravitational acceleration to αg virtually in TIDE, as indicated by Eq. (19). Since α is less than unity (0.88 in our settings), the phase velocity of shallow gravitational waves ($\sqrt{\alpha g/H}$) becomes slower. This mechanism may contribute to reproducibility of the tidal phase.

The reproducibility of the tidal height is evaluated quantitatively here. For this purpose, a root-mean-squared error of η_t, η_{RMSE}, is calculated using η_t^a as a reference (Fig. 5),

$$\eta_{\mathrm{RMSE}} \equiv \left(\frac{1}{T_1 - T_0} \int_{T_0}^{T_1} (\eta_t - \eta_t^a)^2 dt \right)^{1/2} . \tag{25}$$

In TIDE, η_{RMSE} is less than 20 cm even in the open oceans where η_{RMS} is large, and less than 10 cm in most of other regions except for around the Antarctic continent. Meanwhile, in TIDEa1, η_{RMSE} is more than 20 cm in most regions such that it reaches values comparable to η_{RMS} itself.

As in Arbic et al. (2004), who developed a highly-tuned two-layer tide prediction model without a data assimilation technique, the root-mean-square error is averaged over the region ranging from 66°S to 66°N with water depth exceeding 1000 m, which is indicated by 'A',

$$\overline{\eta}_{\mathrm{RMSE}} \equiv \left(\frac{1}{A} \int\int_A \eta_{\mathrm{RMSE}}^2 dx dy \right)^{1/2} . \tag{26}$$

The value is up to 31.3cm in TIDEa1, while 10.0cm in TIDE, which is comparable to 8.9cm in Arbic et al. (2004) (Table 2). In addition, Arbic et al. (2004) defined ”a percentage of SSH variance captured” by $1-(\overline{\eta}_{\mathrm{RMSE}}/\overline{\eta}^{a}_{\mathrm{RMS}})^2$, where $\overline{\eta}^{a}_{\mathrm{RMS}}=31.8$cm is η^{a}_{RMS} averaged over A. The values are 90% in TIDE, 2% in TIDEa1, and 92% in Arbic et al. (2004). The tide reproducibility is very low in TIDEa1, while it increases in TIDE to the same level as a tuned tide model, due to taking into account an approximation of the SAL term. Since a simple viscosity parameterization was used in the experiment, the reproducibility could increase further by adopting more sophisticated parameterizations or tuning the settings more carefully. Though this task is beyond the scope of this paper, some case studies shown in Sect. 3.2 indicate that the tide reproducibility significantly depends on the viscosity settings.

To simulate circulations affected by tides, it is important to introduce tides realistically into an OGCM even in coastal areas (e.g. Moon et al., 2010; Kurapov et al., 2010). However, the reproducibility of the tidal heights tended to decrease there in our low-resolution model. The root-mean-squared error η_{RMSE} averaged over the region shallower than 1000 m is found to be 35.6 cm, which is three times as large as 10.0 cm in the open ocean, and the percentage of SSH variance captured is only 42 % (Table 2). This is likely because our low-resolution model cannot represent relatively small physical processes affecting on the coastal tides, such as excitement of internal tides over shelf slopes, wave breaking on shelves and friction of complicated topographies (Xing and Davies, 1997; Osborne et al., 2011; Nagai and Hibiya, 2012). Improvement of the coastal tides by incorporation of our scheme to a high-resolution OGCM is a future work.

To verify that an OGCM with our tidal scheme runs stably, long time variations are analyzed here. First, the tidal heights η_t(TIDE) for 8 days are shown in Fig. 6a at the same location as Fig. 4, together with η_t^a. Amplitude modulation induced by neap and spring tides is found to be well reproduced in the model. Figure 6b shows η(TIDE) for one year at the same location. Quasi-stationary undulation of SSH is maintained for one year with fortnightly modulation. As systematic indices of the model stability, the volume-averaged kinetic energy of the barotropic currents $\overline{\mathrm{BKE}}$ and the counterpart of the linear tidal currents $\overline{\mathrm{BKE}}_{lt}$ are calculated by

$$\overline{\mathrm{BKE}} = \frac{1}{V} \iiint_V \frac{1}{2} \left| \frac{\boldsymbol{U}}{H+\eta} \right|^2 dxdydz \tag{27}$$

$$\overline{\mathrm{BKE}}_{lt} = \frac{1}{V} \iiint_V \frac{1}{2} \left| \frac{\boldsymbol{U}_{lt}}{H+\eta} \right|^2 dxdydz, \tag{28}$$

where V indicates the whole region of the model [m^3]. Monotonic increase or decrease of energy is not found in their time series of one year, though fortnightly variation exists (Fig. 6c). It can be concluded that the model runs stably with our tidal scheme at least for one year.

3.2 Tidal motion

In this subsection, tidal motions reproduced by the new tidal scheme are validated using the results of cases M2 and K1. As shown in Fig. 2, most of the tidal height variation was represented by the linear tidal component η_{lt} in our global model. Similarly, barotropic currents with tidal frequencies were almost represented by the linear tidal component $\boldsymbol{U}_{lt}$, and therefore $\boldsymbol{U}_{lt}$ is used to compare with past tide studies. Hereafter, the 100-hour experimental results from 20:00 on 5th day (indicated by T_0) to 0:00 on 10th day (T_1) are used for analysis.

As a first step to validate the tidal currents in cases M2 and K1, Fig. 7 shows the mean speed distributions of the barotropic tidal currents $\overline{|\boldsymbol{u}_{lt}|}^t$ calculated by

$$\overline{|\boldsymbol{u}_{lt}|}^t = \frac{1}{T_1 - T_0} \int_{T_0}^{T_1} \left| \frac{\boldsymbol{U}_{lt}}{H+\eta} \right| dt. \tag{29}$$

For both the M2 and K1 cases, the tidal currents are strong in coastal areas, especially near Great Britain, Ireland and far east Asia. In the M2 case, $\overline{|\boldsymbol{u}_{lt}|}^t$ is large over the Mid Atlantic Ridge, and in the equatorial Pacific. In the K1 case, $\overline{|\boldsymbol{u}_{lt}|}^t$ is large in the Indian Ocean and the North Pacific. These results agree well with Fig. 1 of Müller et al. (2010).

Next, we executed an energy analysis for the M2 tide. Generally, the tide energy is supplied to interior ocean regions, and then transported to narrow coastal regions to be dissipated there. Egbert and Ray (2003) analyzed the path ways of the M2 tide energy based on an assimilation model. Following them, the tide energy flux $\boldsymbol{P}$ and the energy supply W (i.e. the work which the tidal forcing does on the ocean) are estimated for the linear tidal component using

$$\boldsymbol{P} = \frac{1}{T_1 - T_0} \int_{T_0}^{T_1} \boldsymbol{U}_{lt} \eta_{lt} dt \tag{30}$$

$$W = \frac{1}{T_1 - T_0} \int_{T_0}^{T_1} \boldsymbol{U}_{lt} \cdot \nabla(\beta \eta_0 + \eta_{\mathrm{SAL}}) dt. \tag{31}$$

Assuming a steady energy state, the energy dissipation D can be estimated from the energy balance as

$$0 = W - \nabla \cdot \boldsymbol{P} - D. \tag{32}$$

See Sect. 3.1 of Egbert and Ray (2001) for their derivation. Figure 8 verifies that the energy was supplied in interior regions, transported to coastal regions, and dissipated there. In addition, the $\boldsymbol{P}$ vector map agrees well with Egbert and Ray (2001). These results indicate that our model reproduced both the tidal heights and the tidal dynamics such as the tidal currents and the energy flux, which are important for effects on the basic fields. Figure 8b shows that the tidal energy dissipates over rough topographies such as the Izu-Ogasawara Ridge, the Hawaiian Ridge and the Central Atlantic Ridge, as well as in coastal regions. This likely reflects barotropic to baroclinic conversion resulting from excitement of internal tides over rough topographies (see Sect. 3.3).

It has been shown that precision of a tide model depends primarily on settings of viscosity and friction to dissipate tidal currents (Arbic et al., 2004). Also in our model experiments, tides significantly depended on the viscosity settings, especially the horizontal viscosity ν. Figure 9 shows η_t in the two additional cases where ν was decreased to 2×10^4 m^2 s^{-1} (case M2v2) and increased to 10×10^4 m^2 s^{-1} (M2v10), together with the standard case with $\nu=6\times10^4$ m^2 s^{-1}. Though the patterns of sea surface elevation were similar, the magnitudes differed significantly, e.g. the local maxima in the eastern equatorial Pacific of 84cm, 63cm and 52cm in cases M2v2, M2 and M2v10, respectively. In addition, it was revealed that the amplitudes of tidal height variation were mainly controlled by the viscosity on the lateral boundary of bottom topography, rather than on the interior currents or bottom friction (not shown). These results are consistent with Schwiderski (1980) and Arbic et al. (2004), who reported that interaction between tidal currents and bottom topography is one of the most important processes in dissipation of tides. As noted here, by using the new scheme, we could adjust the tide viscosity and friction parameters including interaction between tides and topography, without altering the original OGCM equations. This feature is essential to introduce tides into OGCM realistically, as Arbic et al. (2010) pointed out.

3.3 Effects on basic fields

As noted in Sect. 2.2, our new tidal scheme is designed so that interaction processes between the basic fields and tides are represented in the original OGCM framework. Owing to this, the tidal effects on the basic fields would be reproduced naturally in the model, as long as the tidal currents are generated realistically by the scheme. Therefore, we expected that some changes would occur in the velocity and tracer fields of the test experiments, since the tidal currents were well reproduced. In order to validate impacts of our tidal scheme, changes in the basic fields are summarized briefly in this subsection, though the experimental period (40 days) and the model resolution ($1^\circ\times$ $1/2^\circ$) are not enough to represent thorough modification of the basic fields in the real ocean.

In general, active excitement of internal waves is one of the main impacts of tides on the basic fields. Figure 10 shows vertical velocity w at the depth of 1900 m in cases TIDE and NOTIDE. In NOTIDE, with the exception of the equatorial region, w was $\mathrm{O}(10^{-3})$ cm s^{-1}, while w in TIDE was more than 10^{-2} cm s^{-1} over large areas. This difference indicates excitement of internal tides in TIDE. In fact, the vertical velocity was especially large over rough topographies such as the Emperor Seamount Chain (near 170 °E), the Hawaiian Ridge and the Izu-Ogasawara Ridge (140 °E), suggesting active excitement due to interaction between tides and topographies. This is consistent with the energy dissipation D in Fig. 8b

Figure 10 shows that w had a zonal band pattern with a meridional wavelength of approximately 200 km. This pattern is very similar to the result of Komori et al. (2008) (their Fig. 1), who simulated excitement of internal waves by wind using a model with a horizontal resolution of 1/4 °. However, Arbic et al. (2010) reported that internal tides have a ripple-like pattern spreading from bottom topographies, using an eddy-resolving model with a horizontal resolution of approximately 1/10 °. Since reproducibility of internal tides depends sharply on model resolution (Niwa and Hibiya, 2011), this difference suggests that our model resolution of 1 °$\times$ 1/2 °was not enough to represent internal tides.

To examine how the internal tides are excited in the model in more detail, potential density σ_0 is analyzed around Hawaii, where active excitement is expected from the w distribution (Fig. 10). Figure 11a shows time variation of σ_0 vertical distribution in TIDE and NOTIDE. No remarkable variation is found in NOTIDE (thin lines), while vertical undulation of the isopycnals with a period of half a day is clearly seen (thick lines). The amplitude reaches 50 m, which means that the model represented heaving of the isopycnals accompanied with internal tides. Figure 11b is a Hovmöller diagram showing meridional and temporal change of potential density anomaly σ_0' at the depth of 1000 m in TIDE, and σ_0' is the anomaly from the time average as

$$\sigma_0' = \sigma_0 - \frac{1}{T_1 - T_0} \int_{T_0}^{T_1} \sigma_0 dt, \tag{33}$$

where T_0 and T_1 indicate 18 Jun 2001, 0:00 and 20 Jun, 0:00, respectively. In Fig. 11b, σ_0' changed most strongly over the rough topography around Hawaii ($\sim$ 21 °N), showing oscillation with a period of half a day. And then, the anomaly propagated northward and southward with decay (the arrows in the figure). Though the model meridional resolution of 0.5 °is clearly insufficient to represent the spatial structure of the internal tides, it can be concluded that excitement and propagation of the internal tides were represented to some extent.

As another impact on the ocean, Fig. 12a shows sea surface temperature (SST) anomaly $\Delta\overline{T}^t$,

$$\Delta\overline{T}^t = \overline{T}^t(\mathrm{TIDE}) - \overline{T}^t(\mathrm{NOTIDE}), \tag{34}$$

where $\overline{T}^t$ indicates the last 25-hour mean temperature (in 19 June). Introduction of tides resulted in a SST decrease of 0.1-0.5°C over large areas of the Northern Hemisphere. As shown by a vertical temperature profile (Fig. 12b), the surface layer (0-15m) became cooler, while the subsurface layer (20-40m) became warmer, and the temperature stratification was weakened. That is, development of the thermocline in subtropical and subpolar regions of the Northern Hemisphere during its summertime was hampered, and as a result, SST increase in early summer was weakened. This is likely attributed to the process that vertical shear in internal tides feeds vertical mixing in the surface layer through the vertical mixing scheme. The mixing scheme only intermittently predicted large vertical diffusivities. In contrast, $\Delta\overline{T}^t$ was relatively small in the Southern Hemisphere's winter. It is thought that tidal mixing hardly affected the vertical temperature distribution there, since the surface layer was originally well-mixed via surface cooling. Both of temperature and salinity were almost uniform from the surface to the depth of 80m.

The SST decrease with the inclusion of tides was especially large in shallow coastal regions; e.g., more than 1°C around the islands of Great Britain and Ireland. Since this decrease was accompanied with weakening of stratification, the reason is likely that strong tidal currents (Fig. 7) induced vertical mixing through shear instability in the bottom layer, as reported by observational and numerical studies about tidal fronts (Simpson and Hunter, 1974; Müller et al., 2010). The SST anomaly was also large in some polar coastal seas such as the Greenland Sea and the Ross Sea. This is consistent with the findings of previous studies, which showed significant tidal impacts on dense water formation processes there (Pereira et al., 2002; Robertson, 2001a,b).

Our experiment of 40 days did not show any significant changes in large scale circulations. The differences between the currents in TIDE and NOTIDE were less than 1 cm s^{-1} in the open oceans, and 10 cm s^{-1} at maximum in coastal areas (not shown). This result is consistent with a study about tidal effects (Bessiéres et al., 2008), which suggests that our tidal scheme did not generate spurious currents. However, considering the report that tidal mixing modified the Atlantic North Current pathway in a long-term integration of a climate model (Müller et al., 2010), tidal impacts on large scale circulations may appear if we run the model much longer. (In our one-year experiment, the velocity difference between TIDE and NOTIDE reached approximately 10 % of the total velocity in two months. However, it did not expand further after that.)

Though plausible impacts on the OGCM were obtained by our scheme as for impacts of tidal currents, it should be noted that our experiment is preliminary. In particular, the horizontal resolution of the model is too low to represent internal tides or tidal mixing processes (Matsumoto et al., 2000). A thorough investigation is necessary about the process for tidal currents to intensify vertical mixing through velocity shear and turbulence. We plan to execute a long experiment in order to examine the tidal impacts in more detail, including dependencies on model resolution or mixing parameterizations.

4 Conclusions

A new practical scheme is proposed to introduce tides explicitly into ocean general circulation models (OGCMs). In this scheme, barotropic linear response to the tidal forcing is calculated by the time differential equations modified for ocean tides, instead of the original barotropic equations of the OGCM. This allows usage of various parameterizations specified for tides, such as the self attraction / loading (SAL) effect and energy dissipation due to internal tides, without unintentional violation of the original dynamical balances in an OGCM. Owing to this feature, the knowledge of barotropic tide modeling can be exploited to improve reproducibility of tides in an OGCM. In other words, this scheme drives an OGCM by the barotropic tidal currents which are predicted progressively by a tuned tide model, in lieu of using the equilibrium tidal potential. The numerical cost of the scheme is comparable to the barotropic calculation of the original OGCM.

We incorporated this scheme into Meteorological Research Institute Community Ocean Model (MRI.COM) and executed test experiments with a low-resolution global model ($1^\circ \times 1/2^\circ$). The results showed that the model could simulate tides realistically without affecting the basic fields unintentionally, and that the model runs stably for one year at least. The root-mean-squared error of the tidal heights was only 10.0 cm in the reference of a data-assimilation result, suggesting that the tide reproducibility is comparable to that of tide models tuned elaborately. In contrast, in the case that the SAL term was ignored, the reproducibility decreased significantly, as the error was up to 31.3 cm. This suggests that the SAL scalar parameterization must be utilized in order to introduce tides into an OGCM realistically. Although this statement has been pointed out by Arbic et al. (2010), our methodology is different from theirs.

It should be noted that our model settings were rather crude. Recently, sophisticated parameterizations for tidal energy dissipation have been proposed by studies about interaction between tides and topography (e.g. Jayne and St. Laurent, 2001). The tide reproducibility may improve further by adopting such parameterizations, making use of the feature that the tide settings can be decided independently of which OGCM is used. Actually, our case studies showed that the reproducibility depends sharply on the configuration of the viscosity related to topography, suggesting a possible contribution of such parameterizations.

In spite of the crude settings, our model generally reproduced similar amplitudes of the M2 and K1 tidal currents and the tidal energy conversions when compared with previous tidal modeling studies. In addition, excitement of internal tides and enhancement of vertical mixing were found in the model, though the experimental period was as short as 40 days. We did this by generating the realistic tidal currents in the model through an explicit tidal scheme, in contrast to the indirect parameterizations of tidal mixing used by many traditional OGCMs, such as additional increase of the background vertical diffusivity. Usage of our scheme is expected to improve representation of various physical processes such as water exchange between coastal and open oceans, and even chemical and biological processes (e.g. Sect. 8.6 of Simpson and Sharples, 2012). Explicit introduction of tides into an OGCM is a significant step toward upgrade of ocean modeling. We have a plan to investigate the impacts in more detail using a model with a finer resolution.

Appendix A

Modification of tides

Tides affect the basic field as shown in Section 3.3, and in turn, the basic field modifies the tides. For example, when density stratification exists, kinetic energy conversion occurs from barotropic tides to internal tides. In the new tide scheme, the linear tidal component represents the primary barotropic response to the equilibrium tide potential, and does not include such modification. This appendix explains how such modification is represented in the framework of the new tide scheme.

To treat the question clearly and analytically, we consider a simple situation as follows. The ocean state is thoroughly horizontally uniform including the tidal forcing, and dissipation and bottom friction are ignored. Under these assumptions, the momentum equation of the linear tidal component, Eq. (11), is simplified as

$$\frac{\partial U_{lt}}{\partial t} - fV_{lt} = gH\beta\frac{\partial \eta_0}{\partial x} \tag{A1}$$

$$\frac{\partial V_{lt}}{\partial t} + fU_{lt} = gH\beta\frac{\partial \eta_0}{\partial y}. \tag{A2}$$

Now, introducing complex number expressions

$$\boldsymbol{U}_{lt} = U_{lt} + iV_{lt} \tag{A3}$$

$$\boldsymbol{F} = \frac{\partial \eta_0}{\partial x} + i\frac{\partial \eta_0}{\partial y}, \tag{A4}$$

we deform Eqs. (A1) and (A2) into

$$\frac{\partial \boldsymbol{U}_{lt}}{\partial t} + if\boldsymbol{U}_{lt} = gH\beta\boldsymbol{F}. \tag{A5}$$

We assume a horizontal vector varying trigonometrically with frequency σ for the tidal forcing $\boldsymbol{F}$, and as a result, each of $\boldsymbol{U}_{lt}$ and $\boldsymbol{F}$ can be deformed to a sum of the two circular components in general as follows (Davies, 1985; Sakamoto and Akitomo, 2006)

$$\boldsymbol{U}_{lt} = R_{lt}^{+} e^{i\sigma t} + R_{lt}^{-} e^{-i\sigma t} \tag{A6}$$

$$\boldsymbol{F} = F^{+} e^{i\sigma t} + F^{-} e^{-i\sigma t}, \tag{A7}$$

where R_{lt}^{+} and F^{+} are the amplitudes of the anti-clockwise components while R_{lt}^{-} and F^{-} are those of the clockwise components. Substituting Eqs. (A6) and (A7) into Eq. (A5), we obtain the solution of $\boldsymbol{U}_{lt}$ for $\boldsymbol{F}$,

$$R_{lt}^{+} = \frac{gH\beta}{i(\sigma + f)} F^{+} \tag{A8}$$

$$R_{lt}^{-} = \frac{gH\beta}{i(-\sigma + f)} F^{-}. \tag{A9}$$

Now that the solution for the linear tidal component is obtained, we show how the basic equations represent modification of tides induced by secondary interactions between the linear tidal component $\boldsymbol{U}_{lt}$ and the basic field. Making use of the assumptions of Eqs. (A1) and (A2), the barotropic momentum equation of the basic component Eq.(13), i.e. the original equation of OGCM , is simplified to

$$\frac{\partial \boldsymbol{U}_b}{\partial t} + if\boldsymbol{U}_b = \boldsymbol{X}, \tag{A10}$$

where $\boldsymbol{U}_b$ is a complex number,

$$\boldsymbol{U}_b = U_b + iV_b, \tag{A11}$$

and $\boldsymbol{X}$ represents the secondary interactions. Here, we assume a linear damping for $\boldsymbol{X}$. Modeling the barotropic tides as dissipated by excitation of the internal tides due to a combination of tidal currents and stratification,

$$\boldsymbol{X} = -a\boldsymbol{U}_{lt}. \tag{A12}$$

The constant a is a damping coefficient with units of s^{-1}. Now, we deform $\boldsymbol{U}_b$ to a sum of the two circular components in the same manner as Eq. (A6) to give

$$\boldsymbol{U}_b = R_b^+ e^{i\sigma t} + R_b^- e^{-i\sigma t}. \tag{A13}$$

Substituting Eqs. (A12) and (A13) into Eq. (A10), we obtain a modification of the tidal currents induced by the secondary interaction, $\boldsymbol{X}$, to be

$$R_b^+ = \frac{-a}{i(\sigma + f)} R_{lt}^+ \tag{A14}$$

$$R_b^- = \frac{-a}{i(-\sigma + f)} R_{lt}^-. \tag{A15}$$

The actual tidal currents are a sum of the linear tidal component $\boldsymbol{U}_{lt}$ and the modification due to the secondary interactions. Since the latter is equal to $\boldsymbol{U}_b$ in the present situation, the entire tidal currents driven by the forcing $\boldsymbol{F}$ are given by Eqs. (A8), (A9), (A14) and (A15) as follows

$$\begin{aligned}\boldsymbol{U}_{lt} + \boldsymbol{U}_b = &\left(1 + \frac{-a}{i(\sigma + f)}\right) \frac{gH\beta}{i(\sigma + f)} F^+ e^{i\sigma t} \\ &+ \left(1 + \frac{-a}{i(-\sigma + f)}\right) \frac{gH\beta}{i(-\sigma + f)} F^- e^{-i\sigma t}.\end{aligned} \tag{A16}$$

This expression clearly shows how the tidal currents induced by F^+ and F^- are modified by the dumping a, which represents the secondary interaction between the tidal and basic fields. The relative magnitude of the modification against the linear tidal component is indicated by the ratio of a against $\sigma + f$. This means that the modification is usually smaller than the linear tidal component, since time scales of decay of barotropic tidal currents due to excitement of internal waves (or other interaction processes) are usually larger than periods of main tidal constituents or the inertial period ($\sim$ day). This is consistent with our test experiments, where the tides are almost entirely represented by the linear tidal component (Fig. 2).

As explained here using a simple situation, the interaction between the tidal and basic fields emerges through a driving term ($\boldsymbol{X}$) in the basic equation. Change of the basic field induced by

$\boldsymbol{X}$ can be considered as modification of tides if its frequency is the same as the tidal forcing. Otherwise, the change is an excitation of other tidal constituents such as overtides, or modification of the basic field. In any case, these modification processes are represented explicitly in the framework of the original OGCM, although the governing equations of the modification currents $\boldsymbol{U}_b$ are different from those of the linear tidal currents $\boldsymbol{U}_{lt}$.

Acknowledgements. We thank the members of oceanographic research department of Meteorological Research Institute for fruitful discussions and helpful comments. This work was funded by MRI and was partly supported by JSPS KAKENHI Grant Number 24740323.

References

Arbic, B. K., Garner, S. T., Hallberg, R. W., and Simmons, H. L.: The accuracy of surface elevations in forward global barotropic and baroclinic tide models, Deep-Sea Res. II, 51, 3069–3101, doi:10.1016/j.dsr2.2004.09.014, 2004.

Arbic, B. K., Wallcraft, A. J., and Metzger, E. J.: Concurrent simulation of the eddying general circulation and tides in a global ocean model, Ocean Modell., 32, 175–187, doi:10.1016/j.ocemod.2010.01.007, 2010.

Bessiéres, L., Madec, G., and Lyard, F.: Global tidal residual mean circulation: Does it affect a climate OGCM?, Geophys. Res. Lett., 35, L03 609, doi:10.1029/2007GL032644, 2008.

Davies, A. M.: On determining current profiles in oscillatory flows, Appl. Math. Modelling, 9, 419–428, 1985.

Egbert, G. D. and Ray, R. D.: Estimates of M2 tidal energy dissipation from TOPEX/Poseidon altimeter data, J. Geophys. Res., 106, 22 475–22 502, doi:10.1029/2000JC000699, 2001.

Egbert, G. D. and Ray, R. D.: Semi-diurnal and diurnal tidal dissipation from TOPEX/Poseidon altimetry, Geophys. Res. Lett., 30, 1907, doi:10.1029/2003GL017676, 2003.

Griffies, S. M. and Hallberg, R. W.: Biharmonic friction with a Smagorinsky-like viscosity for use in large-scale eddy-permitting ocean models, Mon. Wea. Rev., 128, 2935–2946, 2000.

Griffies, S. M., Biastoch, A., Böning, C., Bryan, F., Danabasoglu, G., Chassignet, E. P., England, M. H., Gerdes, R., Haak, H., Hallberg, R. W., Hazeleger, W., Jungclaus, J., Large, W. G., Madec, G., Pirani, A., Samuels, B. L., Scheinert, M., Gupta, A. S., Severijns, C. A., Simmons, H. L., Treguier, A. M., Winton, M., Yeager, S., and Yin, J.: Coordinated Ocean-ice Reference Experiments (COREs), Ocean Modell., 26, 1–26, 2009.

Hendershott, M. C.: The effects of solid earth deformation on global ocean tides, Gyophys. J. R. Astr. Soc., 29, 389–402, 1972.

Hunke, E. C. and Ducowicz, J. K.: An elastic-viscous-plastic model for sea ice dynamics, J. Phys. Oceanogr., 27, 1849–1867, 1997.

Hunke, E. C. and Ducowicz, J. K.: The elastic-viscous-plastic sea ice dynamics model in general orthogonal curvilinear coordinates on a sphere: Incorporation of metric terms, Mon. Wea. Rev., 130, 1848–1865, 2002.

Jayne, S. R. and St. Laurent, L. C.: Parameterizing tidal dissipation over rough topography, Geophys. Res. Lett., 28, 811–814, 2001.

Kantha, L. H. and Clayson, C. A.: Numerical Models of Oceans and Oceanic Processes, Academic Press, 2000.

Komori, N., Ohfuchi, W., Taguchi, B., Sasaki, H., and Klein, P.: Deep ocean inertia-gravity waves simulated in a high-resolution global coupled atmosphere-ocean GCM, Geophys. Res. Lett., 35, L04 610, doi:10.1029/2007GL032807, 2008.

Kurapov, A. L., Allen, J. S., and Egbert, G. D.: Combined effects of wind-driven upwelling and internal tide on the continental shelf, J. Phys. Oceanogr., 40, 737–756, 2010.

Large, W. G. and Yeager, S. G.: Diurnal to decadal global forcing for coean and sea-ice models: The data sets and flux climatologies, NCAR Tech. Note: TN-460+STR, CGD Division of the Natinal Center for Atmospheric Research, 2004.

Lee, H. C., Rosati, A., and Spelman, M. J.: Barotropic tidal mixing effects in a coupled climate model: Oceanic conditions in the Northern Atlantic, Ocean Modell., 11, 464–477, 2006.

Matsumoto, K., Takanezawa, T., and Ooe, N.: Ocean tide models developed by assimilating TOPEX/POSEIDON altimeter data into hydrodynamical model: A global model and a regional model around Japan, J. Oceanogr., 56, 567–581, 2000.

Mellor, G. L. and Kantha, L.: An ice-ocean coupled model, J. Geophys. Res., 94, 10 937–10 954, 1989.

Moon, J. H., Hirose, N., Yoon, J. H., and Pang, I. C.: Offshore detachment process of the low-salinity water around Changjiang Bank in the East China Sea, J. Phys. Oceanogr., 40, 1035–1053, 2010.

Müller, M., Haak, H., Jüngclaus, J., Sundermann, J., and Thomas, M.: The effect of ocean tides on a climate model simulation, Ocean Modell., 35, 304–313, doi:10.1016/j.ocemod.2010.09.001, 2010.

Munk, W. and Wunsch, C.: Abyssal recipes II: Energetics of tidal and wind mixing, Deep-Sea Res. I, 45, 1977–2010, 1998.

Murray, R. J.: Explicit generation of orthogonal grids for ocean models, J. Comput. Phys., 126, 251–273, 1996.

Nagai, T. and Hibiya, T.: Numerical simulation of tidally induced eddies in the Bungo Channel: A possible role for sporadic Kuroshio-water intrusion (kyucho), J. Oceanogr., 68, 797–806, 2012.

Nakamura, T. and Awaji, T.: Tidally induced diapycnal mixing in the Kuril Straits and its role in water transformation and transport: A three-dimensional nonhydrostatic model experiment, J. Geophys. Res., 109, C09S07, doi:10.1029/2003JC001850, 2004.

Nakano, H. and Suginohara, N.: Effects of Bottom Boundary Layer parameterization on reproducing deep and bottom waters in a world ocean model, J. Phys. Oceanogr., 32, 1209–1227, 2002.

Niwa, Y. and Hibiya, T.: Estimation of baroclinic tide energy available for deep ocean mixing based on three-dimensional global numerical simulations, J. Oceanogr., 67, 493–502, doi:10.1007/s10872-011-0052-1, 2011.

Osafune, S. and Yasuda, I.: Bidecadal variability in the intermediate waters of the northwestern subarctic Pacific and the Okhotsk Sea in relation to 18.6-year period nodal tidal cycle, J. Geophys. Res., 111, C05 007, doi:10.1029/2005JC003277, 2006.

Osborne, J. J., Kurapov, A. L., Egbert, G. D., and Kosro, P. M.: Spatial and temporal variability of the M2 internal tide generation and propagation on the Oregon Shelf, J. Phys. Oceanogr., 41, 2037–2062, 2011.

Pereira, F. P., Beckmann, A., and Hellmer, H. H.: Tidal mixing in the southern Weddell Sea: Results from a three-dimensional model, J. Phys. Oceanogr., 32, 2151–2170, 2002.

Polzin, K. L.: Mesoscale eddy-internal wave coupling. Part I: Symmetry, wave capture, and results from the Mid-Ocean Dynamics Experiment, J. Phys. Oceanogr., 38, 2556–2574, doi:10.1175/2008JPO3666.1, 2008.

Postlethwaite, C. F., Maqueda, M. A. M., Fouest, V. L., Tattersall, G. R., Holt, J., and Willmott, A. J.: The effect of tides on dense water formation in Arctic shelf seas, Ocean Sci., 7, 203–217, 2011.

Prather, M. J.: Numerical advection by conservation of second-order moments, J. Geophys. Res., 91, 6671–6681, doi:10.1029/JD091iD06p06671, 1986.

Robertson, R.: Internal tides and baroclinicity in the southern Weddell Sea 1. Model description, J. Geophys. Res., 106, 27 001–27 016, 2001a.

Robertson, R.: Internal tides and baroclinicity in the southern Weddell Sea 2. Effects of the critical latitude and stratification, J. Geophys. Res., 106, 27 017–27 034, 2001b.

Sakamoto, K. and Akitomo, K.: Instabilities of the tidally induced bottom boundary layer in the rotating frame and their mixing effect, Dyn. Atmos. Oceans, 41, 191–211, 2006.

Sakamoto, K. and Akitomo, K.: The tidally induced bottom boundary layer in the rotating frame: Similarity of turbulence, J. Fluid Mech., 615, 1–25, 2008.
Sakamoto, K. and Akitomo, K.: The tidally induced bottom boundary layer in the rotating frame: Development of the turbulent mixed layer under stratification, J. Fluid Mech., 619, 235–259, 2009.
Schiller, A.: Effects of explicit tidal forcing in an OGCM on the water-mass structure and circulation in the Indonesian throughflow region, Ocean Modell., 6, 31–49, 2004.
Schiller, A. and Fiedler, R.: Explicit tidal forcing in an ocean general circulation model, Geophys. Res. Lett., 34, L03 611, 2007.
Schwiderski, E. W.: On charting global ocean tides, Rev. Geophys. Space Phys., 18, 243–268, doi:10.1029/RG018i001p00243, 1980.
Simpson, J. H. and Hunter, J. R.: Fronts in the Irish Sea, Nature, 250, 404–406, 1974.
Simpson, J. H. and Sharples, J.: Introduction to the physical and biological oceanography of shelf seas, Cambridge University Press, 2012.
St. Laurent, L. and Garrett, C.: The role of internal tides in mixing the deep ocean, J. Phys. Oceanogr., 32, 2882–2899, 2002.
Taylor, G. I.: Tidal friction in the Irish Sea, Phil. Trans. R. Soc. Lond. A, 220, 1–33, doi:10.1098/rsta.1920.0001, 1920.
Thomas, M., Jürgen Sündermann, and Maier-Reimer, E.: Consideration of ocean tides in an OGCM and impacts on subseasonal to decadal polar motion excitation, Geophys. Res. Lett., 28, 2457–2460, 2001.
Tsujino, H., Motoi, T., Ishikawa, I., Hirabara, M., Nakano, H., Yamanaka, G., Yasuda, T., and Ishizaki, H.: Reference manual for the Meteorological Research Institute Community Ocean Model (MRI.COM) version 3, Technical reports of the Meteorological Research Institute 59, Meteorological Research Institute, Japan, 2010.
Tsujino, H., Hirabara, M., Nakano, H., Yasuda, T., Motoi, T., and Yamanaka, G.: Simulating present climate of the global ocean-ice system using the Meteorological Research Institute Community Ocean Model (MRI.COM): simulation characteristics and variability in the Pacific sector, J. Oceanogr., 67, 449–479, doi:10.1007/s10872-011-0050-3, 2011.
Umlauf, L. and Burchard, H.: A generic length-scale equation for geophysical turbulence models, J. Marine Res., 61, 235–265, 2003.
Weatherly, G. L., Blumsack, S. L., and Bird, A. A.: On the effect of diurnal tidal currents in determining the thickness of the turbulent Ekman bottom boundary layer, J. Phys. Oceanogr., 10, 297–300, 1980.
Xing, J. and Davies, A. M.: The influence of wind effects upon internal tides in shelf edge regions, J. Phys. Oceanogr., 27, 2100–2125, 1997.

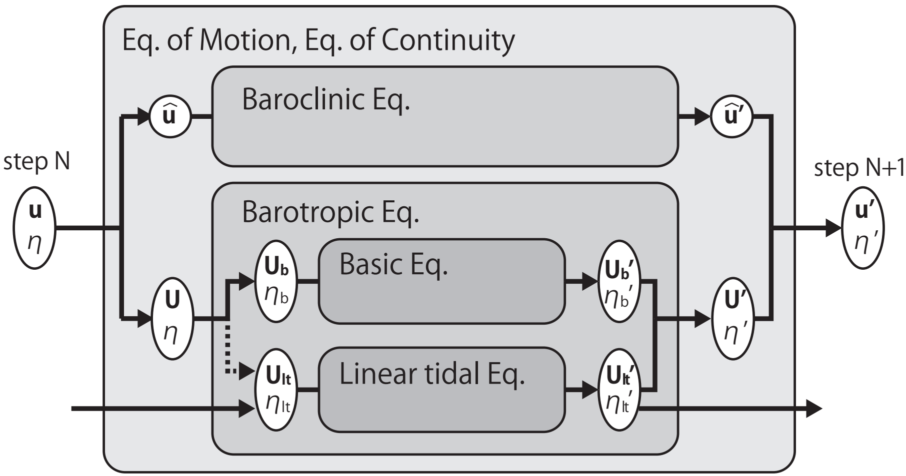

Fig. 1. A schematic view of the calculation procedure of the tide scheme. From $\boldsymbol{u}$ and η at the time step N, $\boldsymbol{u}'$ and η' at the next step $N+1$ are calculated following the equations of motion and continuity. In the calculation process, the mode splitting technique splits the variables into the baroclinic constituent, $\hat{\boldsymbol{u}}$, and the barotropic one, $\boldsymbol{U}$ and η, and then the tide scheme splits the latter into the basic component, $\boldsymbol{U}_b$ and η_b, and the linear tidal component, $\boldsymbol{U}_{lt}$ and η_{lt}. Each component calculates time evolution ($\hat{\boldsymbol{u}}'$,$\boldsymbol{U}_b'$,η_b',$\boldsymbol{U}_{lt}'$ and η_{lt}'), and subsequently all of them are summed to obtain $\boldsymbol{u}'$ and η'. The dashed and solid arrows which point to $\boldsymbol{U}_{lt}$ and η_{lt} mean that their time evolution are given almost independently (see the main text).

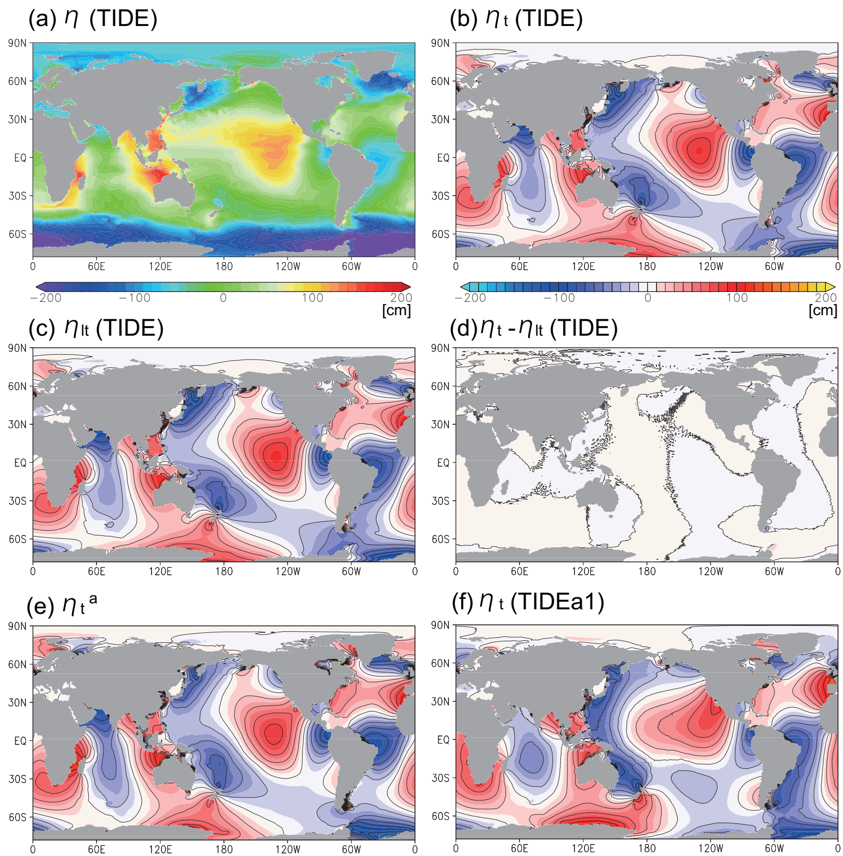

Fig. 2. (a) SSH η, (b) tidal height η_t, (c) height of the linear tidal component η_{lt}, (d) the difference $\eta_t - \eta_{lt}$ in case TIDE, (e) data assimilation analysis η_t^a and (f) η_t in TIDEa1 at the end of the experiments (20 Jun 2001 0:00 UTC). The same color shades are used in (b)-(f), and red indicates ascend (positive) while blue descend (negative). The contour interval is 20 cm.

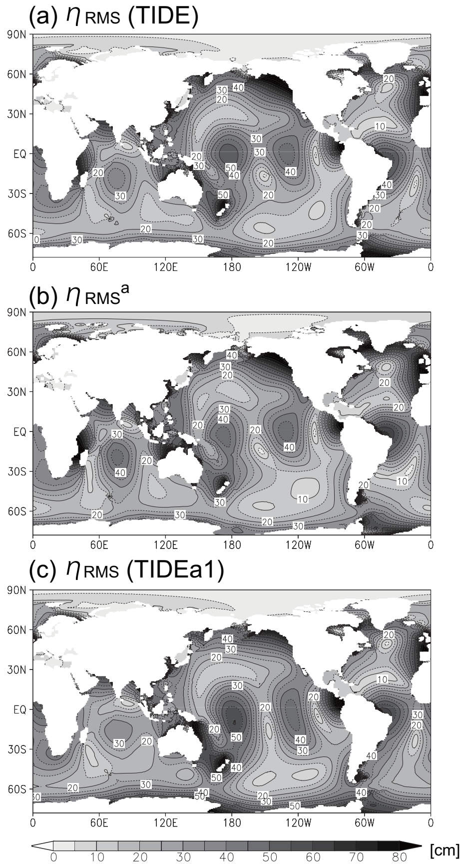

Fig. 3. Root mean square of tidal height η_{RMS} (Eq. 24) in (a) TIDE, (b) assimilation analysis and (c) TIDEa1. The contour interval is 5 cm.

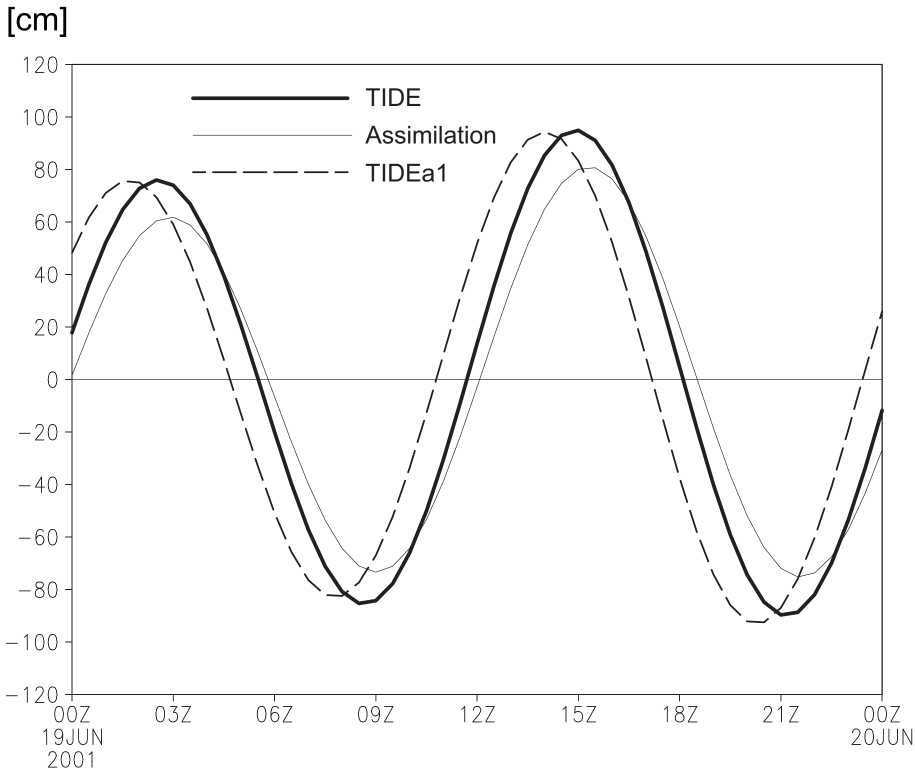

Fig. 4. Time variation of tidal height η_t at the site (180°E, 0°N) for (a) 19-20 Jun 2001 and (b) 12-20 Jun 2001. The thick, thin and dashed lines indicate TIDE, assimilation analysis and TIDEa1, respectively, though TIDEa1 is omitted in (b).

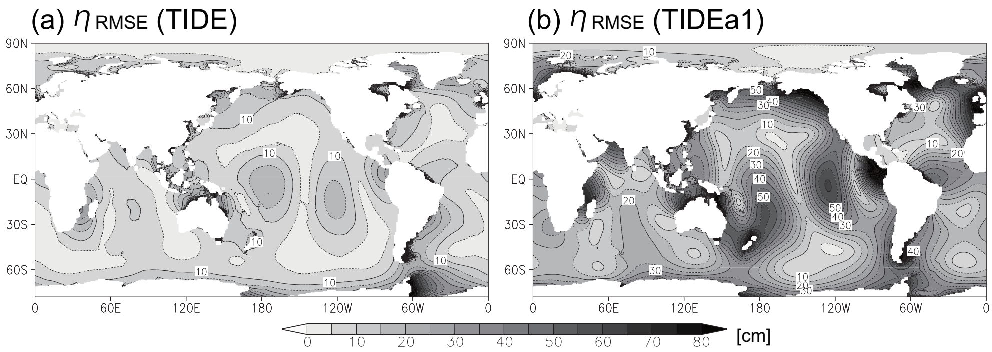

Fig. 5. Root mean square error of the tidal height η_{RMSE} in (a) TIDE and (b) TIDEa1. The contour interval is 5 cm.

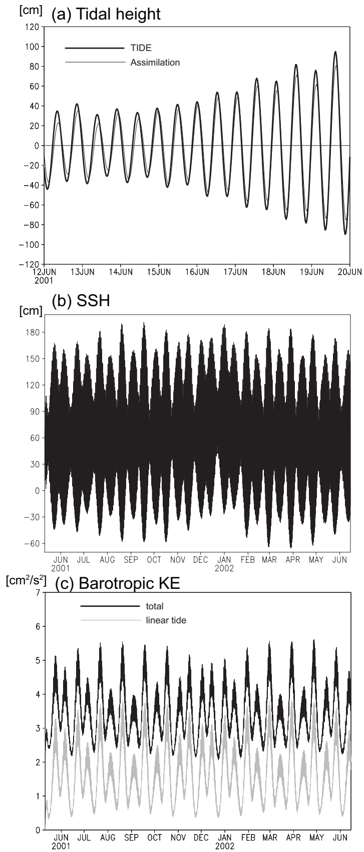

Fig. 6. (a) Same as Fig. 4 but for 12-20 Jun 2001. The thick and thin lines indicate TIDE and assimilation analysis, respectively. (b) One year time variation of SSH at the site (180°E, 0°N) from 21 May 2001 to 20 Jun 2002 in TIDE. (c) Same as (b) but for the volume-averaged barotropic kinetic energy of $\boldsymbol{U}$ ($\overline{\mathrm{BKE}}$, black) and $\boldsymbol{U}_{lt}$ ($\overline{\mathrm{BKE}}_{lt}$,gray).

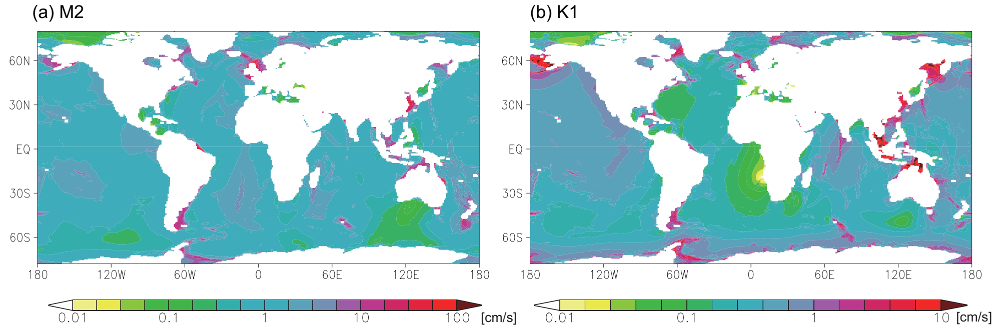

Fig. 7. Mean speed of the barotropic tidal currents $\overline{|\boldsymbol{u}_{lt}|}^{t}$ of (a) M2 tide and (b) K1 tide. The color shades are same as Fig. 1 of Müller et al. (2010), and the units are cm s^{-1}.

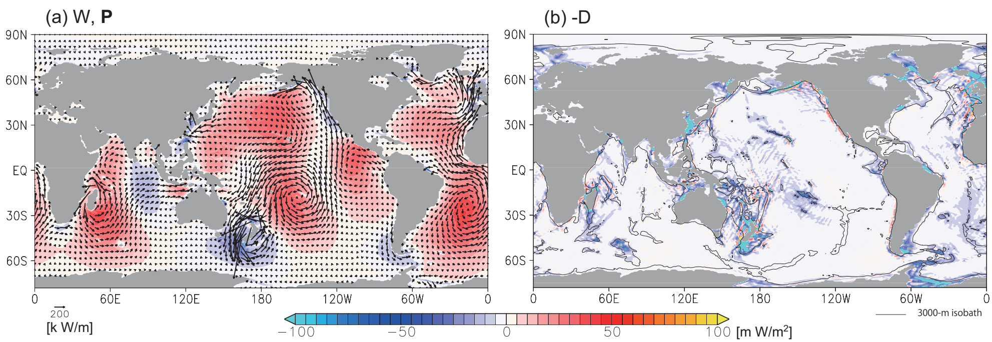

Fig. 8. (a) Tidal energy flux $\boldsymbol{P}$ (vector) and power on the ocean W (color shades) in case M2. The unit length of the vectors is 200 k W m^{-1} the same as Fig. 1 of Egbert and Ray (2001). (b) Tidal energy dissipation $-D$ in case M2. The 3000-m isobath is shown to illustrate the bottom topography.

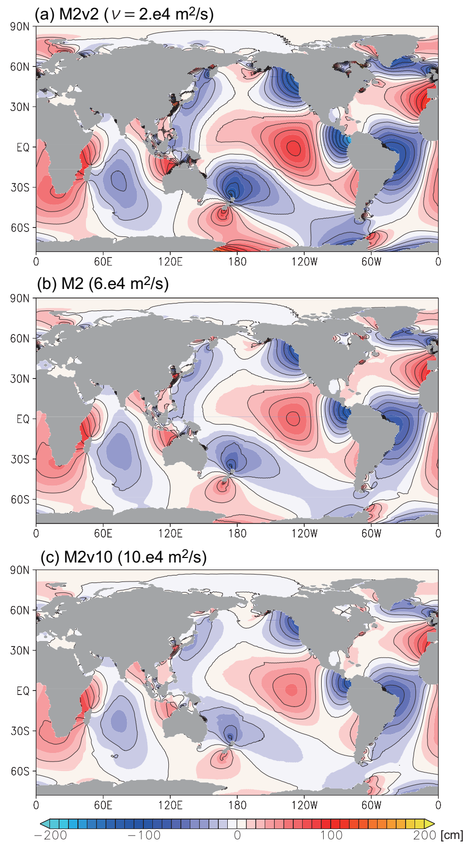

Fig. 9. Tidal height η_t at the end of the experiments (0:00 on 21 May 2001) in cases (a) M2v2 ($\nu = 2 \times 10^4$ m^2 s^{-1}), (b) M2 (6×10^4) and (c) M2v10(10×10^4). The contour interval is 20 cm.

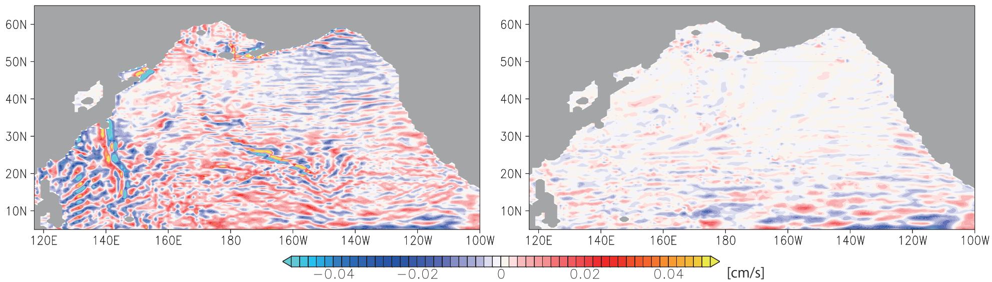

Fig. 10. Vertical velocity w at 1900 m depth in the North Pacific in (a) TIDE and (b) NOTIDE. The instantaneous distributions at the end of the experiment are shown.

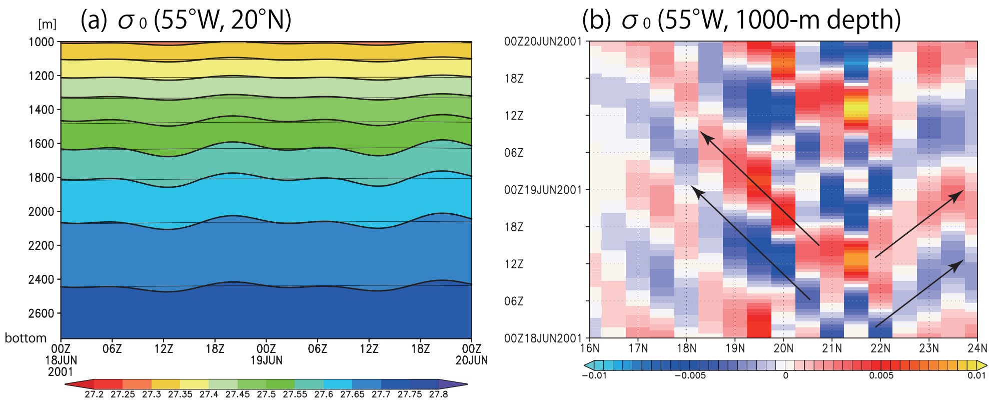

Fig. 11. (a) Vertical distribution of potential density σ_0 from bottom to the 1000-m depth at (55 °W, 20 °N) for 18-20 Jun 2001 of TIDE (thick lines and color shade) and NOTIDE (thin lines). (b) Hovmöller diagram of potential density anomaly σ_0' at 55 °W, 1000-m depth in TIDE. The meridional range is 16-24 °N, and the time period is the same as (a). The arrows indicate propagation of internal tides.

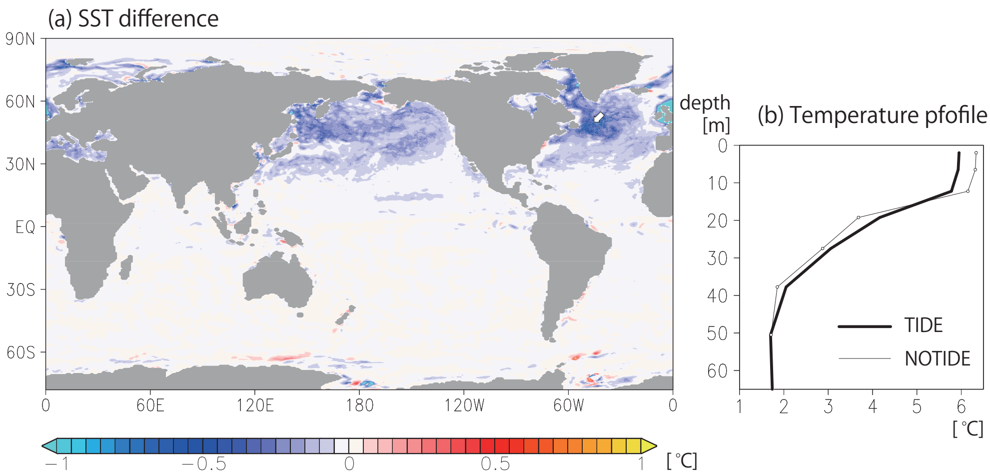

Fig. 12. (a) SST difference between TIDE and NOTIDE $\Delta\overline{T}^t$. (b) Vertical profiles of temperature $\overline{T}^t$ at the site (50° W, 50° N) (marked in (a)) in TIDE (thick line) and NOTIDE (thin). The vertical range from surface to 65 m depth is shown. Both of (a) and (b) use 25-hour averages of the end of the experiments.

Table 1. Experimental cases simulated using our new scheme with MRI.COM.

Abbreviation	settings
NOTIDE	without tides
TIDE	8 tidal constituents
TIDEa1	8 tidal constituents, $\alpha = 1$
M2	M2
K1	K1
M2v2	M2, horizontal viscosity = 2×10^4 m^2 s^{-1}
M2v10	M2, horizontal viscosity = 10×10^4 m^2 s^{-1}

Table 2. Reproducibility of the tidal height in TIDE, TIDEa1 and the tide prediction model of Arbic et al. (2004). The values of 'TIDE(coastal)' are calculated in the region shallower than 1000 m.

Case	TIDE	TIDEa1	Arbic et al. (2004)	TIDE(coastal)
Error RMS [cm]	10.0	31.3	8.9	35.6
percentage of SSH variance captured[%]	90	2	92	42